DESIGN AND EXPERIMENT OF OVERLOAD PROTECTION AND AUTOMATIC OBSTACLE AVOIDANCE MECHANISM FOR BIDIRECTIONAL PLOUGHING EQUIPMENT
/
双向犁耕防过载自动避障机构的设计与试验

Jinbao LIU[1)], Xuan ZHENG[*1)], Yanhui ZHANG[2)], Yuying SONG[2)], Zhihui TANG[1)]

[1)]Machinery Equipment Research Institute, Xinjiang Academy of Agricultural and Reclamation Science, Shihezi, 832000, China

[2)]College of Sciences, Shihezi University, Shihezi, 832000, China

Corresponding authors: Xuan Zheng, E-mail: jiazhengxuan@sohu.com

DOI: https://doi.org/10.35633/inmateh-71-52

***Keywords*: Agricultural engineering; Bidirectional ploughing; Overload protection; Automatic obstacle avoidance; Design; Experiments**

ABSTRACT

During the tillage of two-way ploughing equipment in rocky and barren soil, due to hard objects such as stones, the plough and the key working parts such as plough column are deformed and broken, thereby reducing the reliability and service life of machines and tools. As such, an anti-overload automatic obstacle avoidance mechanism for two-way ploughing is developed. The maximum obstacle avoidance height is 40 cm, and the obstacle avoidance angle α is designed. The rotation range is 4.6~51.5°, and the effective compression stroke of the spring after pre-tightening is 39.34 mm. The motion equation and quasi-static force equation of the mechanism are established. The ploughing resistance in the equilibrium state is 9.74 KN, and the required spring preload is 9.75 KN. Under the safety factor of 1.3, different spring elastic coefficients change with the rotation angle of the mechanism. The virtual prototype simulation model of the anti-overload automatic obstacle avoidance mechanism is established. The simulation results show that the mechanism can effectively perform the obstacle avoidance action. Bench test verifies that the mechanism can avoid obstacles according to the predetermined load. The field test shows that the stability coefficient of the ploughing depth of the mechanism is less than 8%. The results can effectively realize the obstacle avoidance function and ensure the farming quality, and provide an efficient and reliable anti-overload obstacle avoidance structure and parameter basis for the rocky land.

摘要

针对当前双向犁耕装备在多石贫瘠土壤耕作过程中，石块等坚硬物体使犁体以及犁柱等关键工作部件产生变形、断裂，降低了机具可靠性和使用寿命等问题，研制了双向犁耕防过载自动避障机构，对过载保护自动避障机构的结构和关键参数进行了设计，设计最大避障高度为 40cm，避障转角 α 转动范围为 4.6°~51.5°，弹簧预紧后的有效压缩行程为 39.34mm。分别建立了机构运动方程和准静态受力方程，得到平衡状态下犁耕阻力 9.74KN 对应所需的弹簧预紧力为 9.75KN，为提高机构可靠性设置安全系数为 1.3，分析了不同弹簧弹性系数随机构转角 α 的变化曲线。通过台架试验验证了机构能按照预定载荷进行避障动作，进行了田间试验，根据响应曲面设计法中 Box-Behnken Design 原理，试验结果表明，对耕深稳定性变异系数影响的贡献率由大到小依次为：耕速、耕深和弹簧弹性系数。机构耕深稳定性变异系数均小于 8%，能有效实现避障功能并能保证耕作质量，为多石地提供了高效可靠的防过载避障结构和参数依据。

INTRODUCTION

The farming soils in Xinjiang, West China are more barren, harder and more severely salinized than the black soils in Northeast China. Most farmlands are located at mountainous areas or valley basins, adjacent to grasslands, deserts and Gobi *(Wang et al., 2020; Gao et al., 2021)*. Consequently, the soils are rich in stones, fine sands and tree roots. In addition, agricultural machinery tillage will further compact the soil *(Mileusnić et al., 2022; Guilherme et al., 2021)*.

[1] *Jinbao Liu, Associate Researcher; Xuan Zheng, Researcher; Yanhui Zhang, Lecturer; Yuying Song, Postgraduate; Zhihui Tang, Researcher*

Studies have shown that straw manuring, ploughing & deep turning, and other mechanized tillage skills can improve salinized barren soils *(Zhang et al., 2020)*. The requirements for tillage modes and technical equipment have increased. When the existing tillage equipment contacts with hard objects, it will generate a larger load than the soils, resulting in deformation and fracture of the key parts of the plough and plough columns, reducing the working reliability of the whole machine and shortening the service life of the plough *(Li et al., 2021; Liu et al., 2021).*

The uneven resistance generated during ploughing *(Salavat et al., 2023; Kim, 2021, Kim, 2022a; Kim, 2022b)* will have a large impact on the implement *(Sheng et al., 2023; Mileusnić, 2022),* so does the traction performance of tractors *(Yeon et al., 2022; Mojtaba, 2023; Shafaei, 2021).* The anti-overload automatic obstacle avoidance mechanisms in agricultural machinery have been extensively studied. For instance, a bilateral working intra-row automatic obstacle avoidance weeder was designed, which can be used for effective intra-row weeding of grapes cultivated in trellis *(Ma et al., 2020).* An anti-overload flip plough consisting of an obstacle avoidance mechanism, an accumulator and an oil cylinder was designed *(Ma and Chang, 2020). Zhang (2021a)* designed an initiative obstacle avoidance and stubble cutting device for ploughing and stubble cutting in rocky desertification areas of Yunnan, which improved the service life and efficiency of stubble cutting devices. *Zhang et al. (2021b)* designed a boom manipulator obstacle detection system by integrating Beidou and LIDAR, which can acquire the position of obstacles. The two-way plough protectors in engineering applications are usually based on cutting bolts. When in contact with hard obstacles, the cutting bolts fracture and the plough body cannot work, which protects other parts of the plough from damage *(Wittke et al., 2022).* However, after the fracture of cutting bolts, the replacement is time-consuming and labour-intensive, and is more frequent in farmlands with stones, thereby largely reducing the working efficiency. The design of two-way plough equipment for anti-overload automatic obstacle avoidance mechanisms is rarely reported in China.

Herein, a two-way plough equipment with an anti-overload automatic obstacle avoidance mechanism is designed, aiming to solve the problem of rapid response and avoidance of stones when working in stone-rich barren soils. This design can rapidly restore after passing through stones, improving the reliability, adaptively and ploughing efficiency of ploughs. It can also offer a reference for other farming equipment to achieve anti-overload automatic obstacle avoidance, further improving the farming quality in barren soils, creating favourable seedbed conditions for crop growth.

MATERIALS AND METHODS

The anti-overload automatic obstacle avoidance mechanism of flip ploughs mainly consists of fixation boards, hinge shafts, connecting poles, plough column clamps, plough columns, plough body, elastic energy accumulator, supporting poles, and roller wheels. The structural installation is shown in Fig. 1, and the structure of the elastic accumulator is shown in Fig. 2.

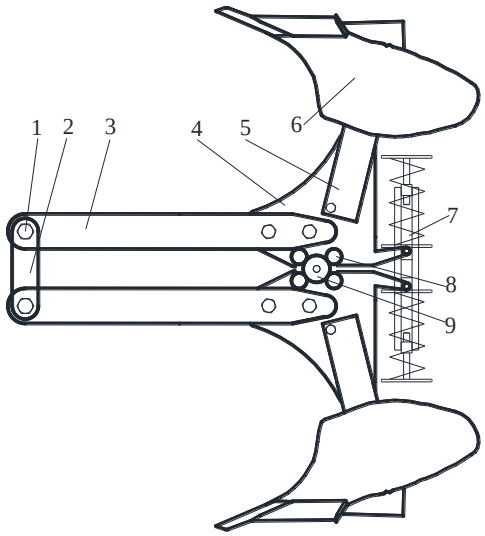

Fig. 1- Structure diagram of the overload protection mechanism

1. hinge shaft; 2. fixation board; 3. connecting pole; 4. plough column clamp; 5. plough column; 6. plough body; 7. elastic accumulator system;8. supporting pole;9. roller column

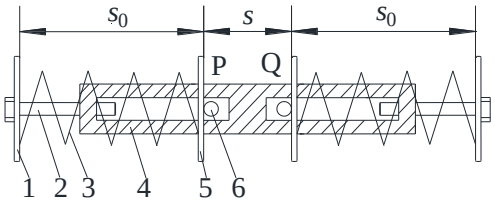

Fig. 2 - Structure diagram of the elastic accumulator

1. Upper seat of spring; 2. regulating pole; 3. spring; 4. spring frame; 5. lower seat of spring; 6. limit pins

For convenient design analysis, it can be taken as a multi-pole mechanism consisting of part 1 (AD1DQI), part 2 (CC1DD1), part 3 (BCC1PI1), part 4 (AB) and elastic accumulator PQ. The elastic accumulator PQ can impose pre-tightening forces at the points P and Q. Figures 3a and 3b shows the normal plough tillage status and the obstacle avoidance status when in contacting with stones respectively.

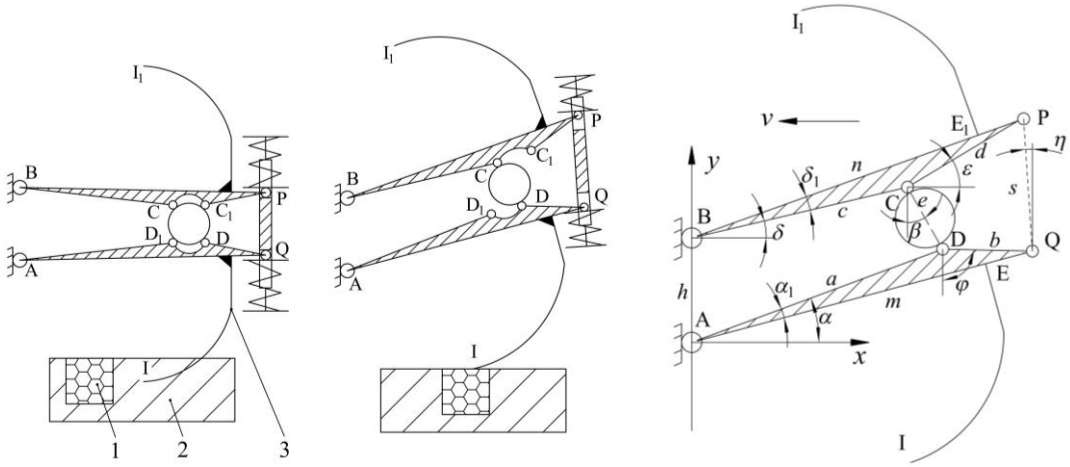

a. Plough tillage status *b. Obstacle avoidance status* *c. Diagram of the mechanism*

Fig. 3 - Diagram of overload protection automatic obstacle avoidance mechanism

1. Rock; 2. Soil; 3. Obstacle avoidance mechanism

In the xAy coordinate system (Fig. 3c), the vector equation in the closed vector polygon ABCDA is *(Naderi-Boldaji et al., 2023; Zhang et al., 2023) as follows:*

$$\left.\begin{aligned} c\cos\delta &= a\cos\alpha - e\sin\beta \\ h + c\sin\delta &= a\sin\alpha + e\cos\beta \end{aligned}\right\} \quad (1)$$

where a – the length of pole AD, mm;

c – the length of pole BC, mm;

e – the supporting diameter of roller, mm;

h – the length of frame AB, mm;

α – the included angle between pole AD and the horizontal direction, (°);

β – the included angle between pole CD and the vertical direction, (°);

δ – the included angle between pole BC and the horizontal direction, (°).

The coordinates of points P and Q are as follows:

$$\left.\begin{aligned} x_P &= n\cos(\delta+\delta_1) \\ y_P &= h + n\sin(\delta+\delta_1) \end{aligned}\right\} \quad (2)$$

$$\left.\begin{aligned} x_Q &= m\cos(\alpha-\alpha_1) \\ y_Q &= m\sin(\alpha-\alpha_1) \end{aligned}\right\} \quad (3)$$

where x_P, and y_P – the coordinates of point P in the xAy coordinate system;

x_Q, and y_Q – the coordinates of point Q in the xAy system;

m – the length of pole AQ, mm;

n – the length of pole BP, mm;

α_1 – the included angle between pole AD and pole AQ, (°);

δ_1 – the included angle between pole BC and pole BP, (°).

Specifically, the pole ADQ and pole BCP constitute a triangle:

$$\left.\begin{aligned}\alpha_1 &= \arccos\frac{a^2+m^2-b^2}{2am}\\ \delta_1 &= \arccos\frac{c^2+n^2-d^2}{2cn}\end{aligned}\right\} \quad (4)$$

where b is the length of pole DQ, mm; d is the length of pole CP, mm.

According to the coordinates of points P and Q, there is:

$$s = \left[(x_P - x_Q)^2 + (y_P - y_Q)^2\right]^{\frac{1}{2}} \quad (5)$$

$$\eta = \arctan\left(\frac{x_Q - x_P}{y_P - y_Q}\right) \quad (6)$$

where s is the distance between the upper and lower limit pins PQ, mm; η is the included angle between elastic accumulator PQ and the vertical direction, (°).

According to the structure of the flip plough, the obstacle avoidance mechanism is preliminarily set as a = 710 mm, b = 88.5 mm, c = 630 mm, d = 158 mm, h = 170 mm, m = 775 mm, n = 775 mm, α_1 = 4.6°, and δ_1 = 5.2°. The supporting diameter e of the roller wheel is 98 mm, and the central angle is θ. When the angle movement range α is 4.6°-90°, the relative changing curves of δ, η and s relative to α can be comprehensively known (Fig. 4).

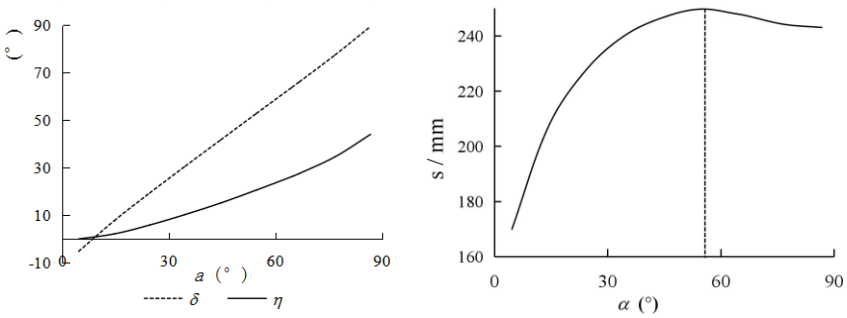

a. Changes of δ and η relative to α b. Changes of s relative to α

Fig. 4 - Change diagram of mechanism motion angle

The actual ploughing depth is usually 25-35 cm. Thus, the obstacle avoidance height is set as Δy_I=40 cm, ensuring the obstacles can be fully passed. Consequently, the angle rotation range is 4.6°-51.5°. The distance s of PQ is 170-248.68 mm. The effective compression stroke Δs of the pre-tensional spring are 39.34mm.

Its statical behaviours are analysed. Figs. 5 (a) and 5(b) show the normal ploughing state, and the anti-overload automatic obstacle avoidance state, respectively.

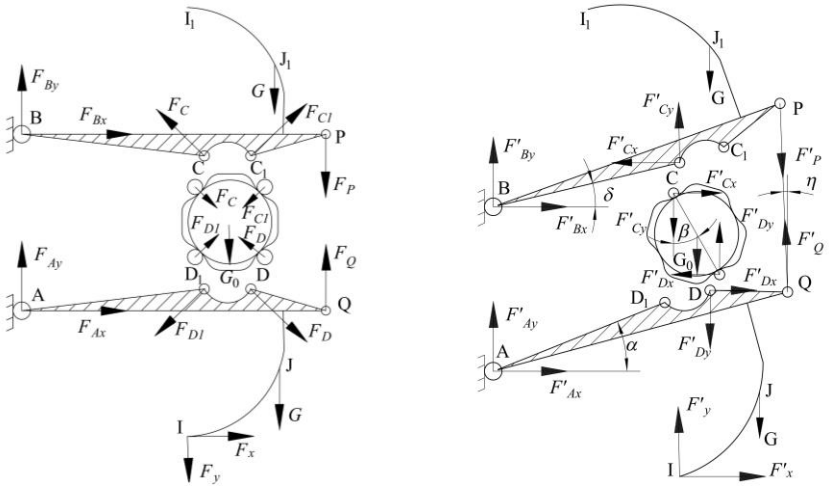

a. Plough tillage status b. Obstacle avoidance status

Fig. 5 - Static analysis diagram of mechanism

According to Figure 5b, the equilibrium equation 7 of the mechanism is obtained by applying force:

$$\left.\begin{aligned}
F'_{Ax}+F'_{Dx}+F'_{x}-F'_{Q}\sin\eta=0\\
F'_{Ay}-F'_{Dy}-F'_{y}-G+F'_{Q}\cos\eta=0\\
F'_{x}\,l\cos\lambda-F'_{y}\,l\sin\lambda-F'_{Dx}\,a\sin\alpha-F'_{Dy}\,a\cos\alpha+\\
F'_{Q}\cos\eta\cdot m\cos(\alpha-\alpha_1)+F'_{Q}\sin\eta\cdot m\sin(\alpha-\alpha_1)\\
-Gl_1\cos(\lambda_1-\alpha)=0\\
F'_{Cx}-F'_{Dx}=0\\
F'_{Dy}+G_0-F'_{Cy}=0\\
F'_{Dx}\,e\cos\beta-F'_{Dy}\,e\sin\beta+G_0\frac{e}{2}\sin\beta=0\\
F'_{Bx}-F'_{Cx}+F'_{P}\sin\eta=0\\
F'_{By}+F'_{Cy}-F'_{P}\cos\eta-G=0\\
F'_{Cx}\,c\sin\delta+F'_{Cy}\,c\cos\delta-F'_{P}\cos\eta\cdot n\cos(\delta+\delta_1)-\\
F'_{P}\sin\eta\cdot n\sin(\delta+\delta_1)-Gl_1\cos(\lambda_1+\delta)=0
\end{aligned}\right\} \quad (7)$$

where F_{Ax}, F_{Ay} – the support reaction forces at hinge point A, N;

F_{Bx}, F_{By} – the support reaction forces at hinge point B, N;

F_C – the support reaction force at supporting point C, N;

F_D – the support reaction force at supporting point D, N;

F_{C1} – the support reaction force at supporting point C1, N;

F_{D1} – the support reaction force at supporting point D1, N;

F_x, F_y – the resistance at centre-of-mass of the plough, N;

F_P, F_Q—the spring force of the elastic accumulator, N;

G – the gravity of upper and lower linkage plough, N;

G_0 – the gravity of roller wheel, N.

l – the distance from centre-of-mass I of the plough to hinge point A, mm;

l_1 – the distance from the assembly centre-of-mass J of the upper-lower linkage - plough to point A, mm;

λ - the included angle between l and the vertical direction, (°);

λ_1 – the included angle between l_1 and the horizontal direction, (°).

A three-dimensional model of the obstacle avoidance mechanism is built on SolidWorks. According to the preliminary parameter setting of the obstacle avoidance mechanism, the weights of part 1 (ADD1QI) and part 3 (BCC1PI1) are measured to be 995 N. When the mechanism is under normal ploughing state, the distance l_1 from the centre-of-mass of part *1* relative to point A is 767.4 mm; the included angle λ_1 relative to the horizontal direction is 27.36°; the distance l from the centre-of-mass I of the plough to hinge point A is 880 mm, and the included angle λ between l and the upright direction is 50°. Under the above conditions, when the ploughing resistance is known, the ranges of the spring initial pre-tightening force and the spring force during compression can be determined.

Based on the reported test methods, the resistance is measured using a developed plough-specific remote collector (Fig. 6). The remote collector connected the plough to the tractor.

Fig. 6 - Field experiments

1. Data collector; 2. Upper hanging sensor; 3. Lower hanging sensor

Figure 7 shows the variation of ploughing resistance in the normal tillage state.

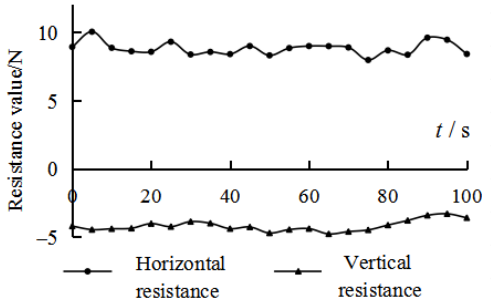

Fig. 7 - Structure and resistance of the plough

The test method at preliminary phase *(Liu et al., 2022)* is adopted, with a tillage speed of 12 km·h^{-1}, a tilling width of 0.42 m and a tillage depth of 0.35 m. The results show that the average horizontal resistance faced by the plough is 8.79 KN, and the average vertical resistance is 4.19 KN. Based on Eq. (7), it has F_P = F_Q = 9.75 KN. At this moment, the combined resistance F_z of the plough is 9.74 KN.

$$F_z = \sqrt{F_x^{\,2} + F_y^{\,2}} \tag{8}$$

The horizontal resistance F_x and vertical resistance F_y of the plough are determined by the plough structure and tillage conditions. The included angle σ between the two is as follows:

$$\tan\sigma = \frac{F_y}{F_x} \tag{9}$$

Based on Eq. (7), the average σ of the plough is 25.45°. The magnitude and direction of the horizontal resistance F_x and the vertical resistance F_y imposed on the plough are largely affected by the spring force F_P. The variation of the plough is shown in Fig. 8. When the combined resistance on the plough is known under the normal tillage state, as the angle σ gradually increases, the corresponding spring force decreases slowly. When σ is greater than 40.07°, the mechanism balance can be maintained only when the spring force direction changes. Thus, a reasonable plough structure cannot only generate minimal tillage resistance, but also require minimal spring force in an equilibrium state.

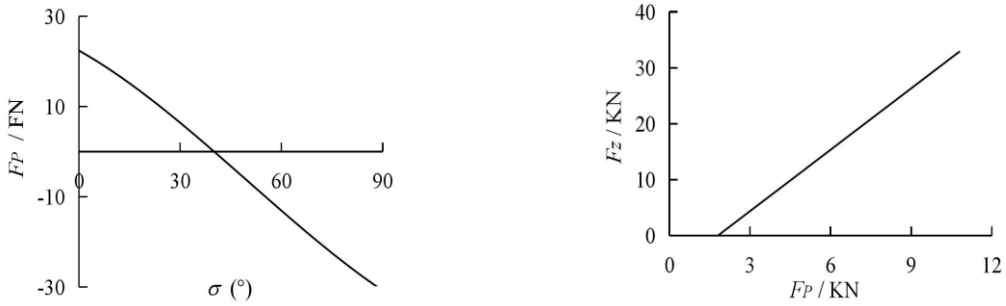

a. Effect of angle σ on spring force b. Relationship between the plough resistance and the spring pre-tightening force

Fig. 8 - Relationship between the plough body and the spring preload

According to the structure of the elastic accumulator, the upper and lower groups of springs are symmetrical, and the spring forces are equal between the two groups at any time. Hence, there is:

$$F_P = F_Q = k(s_1 - s_0) \tag{10}$$

where k – the elasticity coefficient of spring, KN/mm;

s_1 – the original length of spring, mm;

s_0 – the spring length after compression, mm.

After the initial pretension compression, the compression during obstacle avoidance is induced by the enlarged distance between the upper and lower limits. Hence, there is:

$$\frac{\Delta s}{2} = s_1 - s_0 \tag{11}$$

where Δs – the distance change between the upper and lower limit pins, mm.

Based on the preliminary parameter setting and the influence factors on the mechanism movement (auxiliary internal friction force), the safety factor is set as 1.3. The specific rigidity spring and variable rigidity spring are both analysed. The elastic coefficient of the specific rigidity spring is set as a constant. Fig. 9 shows the changes in the spring force with 4 levels of constant rigidity. As α gradually increases during the obstacle avoidance, the centre-of-mass height of the plough increases, and the spring force is enhanced. The smaller the elastic coefficient of the spring, the smaller the increase in spring force.

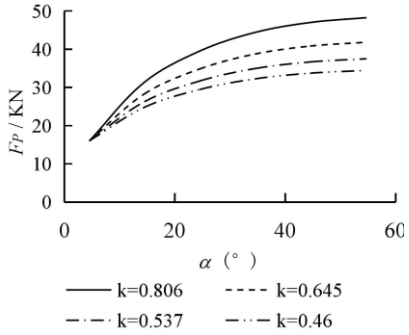

Fig. 9 - Change of spring force

RESULTS AND ANALYSIS

To avoid the effects of relevant structural parameters and motion parameters of the obstacle avoidance mechanism on tillage, the mechanism model is simplified to establish a 3D model on SolidWorks and imported it to ADAMS. Depending on how the parts are connected and moved, restraints are added between different parts (such as fixation pair, rotation pair, or mobile pair). The spring is added into the elastic accumulator, and the actual resistance is added to the centre-of-mass of the plough. During the simulation of obstacle avoidance, a contact force is added between the plough and ground, and the spheres are set on the ground to simulate rock obstacles. The height of the heaves above the ground is 30 cm. A straight-line movement drive is added onto the motion pair of the frame and ground, and the velocities are 2.22, 2.78, 3.33 m/s to simulate the actual working velocity and the mechanism movement from right to left (Fig. 10).

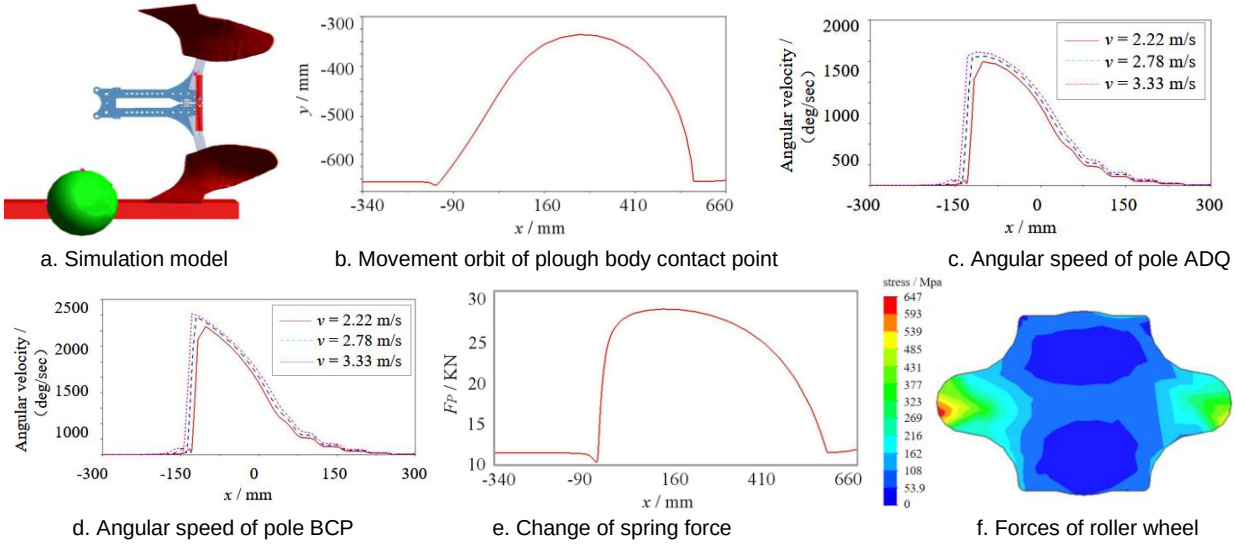

a. Simulation model b. Movement orbit of plough body contact point c. Angular speed of pole ADQ

d. Angular speed of pole BCP e. Change of spring force f. Forces of roller wheel

Fig. 10 - Mechanism simulation analysis

The motion obit of the plough contact point during obstacle avoidance is basically consistent with the contour of the obstacles. The mechanism can effectively avoid the obstacles (Fig. 10). Figs. 10c and 10d show the changes in the angular speeds of poles ADQ and BCP. Clearly, at a fast-working velocity, the obstacle avoidance rotation of the mechanism is fast. The angular speed of mechanism slightly fluctuates after the obstacle avoidance, indicating the working speed will affect the tillage stability to some extent. Moreover, the mechanism, after passing through the obstacles, can return quickly. The simulations show that the mechanism can simulate obstacle avoidance according to the contour of the obstacles. After passing the obstacles, it can restore rapidly, showing excellent obstacle avoidance performance.

The material of the trolley wheels is 40Cr, and the yield strength is 785 MPa. The results show that under a maximum impact load of 1.6 times the actual resistance, the maximum stress faced by the trolley wheels is 647 MPa, and the stress is concentrated on at the edge of contact with the supports.

A test bench is built up (Fig.11). The power supply of pulling force is the horizontal traction of the forklift. In the tests, a pulling force is applied through the forklift to simulate the actual resistance. A digital display pulling force meter is installed between the forklift and the mechanism, which can record the pulling force in real time. The spring coefficient is 0.46 kN/mm.

Fig. 11 – Anti-overload automatic obstacle avoidance test bench

1. Tensile power supply; 2. Digital display pulling force meter; 3. Spring; 4. Anti-overload automatic obstacle avoidance mechanism

The mechanical performance of the mechanism is validated by measuring the pulling force and connecting pole rotation angle on the bench. The tested data are listed in Table 1.

Table 1

Mechanism bench test data

No.	Pulling force /KN	Connecting pole rotation angle /(°)	
		Theoretical value	Tested value
1	15	0	0
2	16.3	0.5	0.2
3	24.8	10	9.5
4	29.5	20	19.7

Testing data comparison and theoretical analysis show that when the resistance is the same, the tested values of the connecting rod rotation angle and spring compression quantity are slightly smaller than the theoretical data. In actual conditions (Fig. 12), the revolving pair and spring seat connected to the connecting pole both generated slight frictional resistance at the hinge sites.

a. Obstacle avoidance rotation 1 *b. Obstacle avoidance rotation 2* *c. Obstacle avoidance limit positions*

d. Relocation dynamics 1 *e. Relocation dynamics 2* *f. Relocation dynamics 3*

Fig. 12 - Test movement process of obstacle avoidance mechanism

Conditions in the test site: the local soil generally contains rocks and gravels. In the 8th company, 164th regiment with rock-rich rocks, the average proportion of rocks in a 1 m^2 space with a tillage depth of 30 cm is 11.8%. The average residual stubble density is 3.6 kg/m^2, and the average water contents in soils with the depths of 0-10 cm, 10-20 cm, and 20-30 cm are 10.15%, 14.2% and 19.78%. The experiments were conducted in September 2021, and the auxiliary power supply was a John Deere 2204 wheeled tractor (Fig. 13).

Since the depth and speed of the plough tillage are the main factors that affect tillage resistance, according to the forces of the obstacle avoidance mechanism, the working stability and reliability of the mechanism shall be improved to make the obstacle avoidance mechanism adapt to different tillage depths and tillage speeds. Hence, the reliability of the machines and tools is determined according to the coefficient of variation of tillage depth stability.

Fig. 13 - Prototype field experiments

To study the effects of machine structure and working parameters on tillage, tillage depth stability is used to effectively reflect the stability of the mechanism under the normal working conditions. The tillage speed, tillage depth and spring elastic coefficient are selected as the testing factors. Taking the coefficient of variation of tillage depth stability as the evaluation index, the level of each factor is determined using the Box-Behnken Design of the response surface method software Design-Expert 8.0.6 (Table 2).

Table 2

Level of test factors

Level	Factor		
	Tillage speed /(m/s)	Tillage depth /cm	Spring elasticity coefficient/(KN/mm)
-1	2.22	25	0.415
0	2.78	30	0.460
1	3.33	35	0.535

Based on Box-Behnken Design, totally 17 groups of experiments were conducted. In each group, 20 measuring points were set and the average value was adopted. Then the variation coefficient of tillage depth stability in each group was determined. The results are shown in Table 3.

Table 3

Results of test

No.	Factor (code)			
	Tillage speed /(m/s)	Tillage depth/cm	Spring elasticity coefficient/(KN/mm)	variation coefficient of tillage depth stability /%
1	1	0	1	5.795
2	-1	0	1	5.135
3	0	1	1	5.021
4	0	0	0	5.97
5	0	0	0	5.755
6	1	0	-1	7.152
7	0	0	0	5.871
8	0	0	0	5.915
9	-1	-1	0	5.353
10	0	-1	1	6.002
11	0	-1	-1	7.125
12	-1	1	0	5.125
13	1	-1	0	6.915
14	1	1	0	5.893
15	0	0	0	5.756
16	-1	0	-1	5.522
17	0	1	-1	5.388

The testing data in Table 5 are sent to fitting and analysis of variance (ANOVA) on Design Expert 8.0.6. Then 2FI regression models of variation coefficient of tillage depth stability is established, and the significance tests of the models are shown in Table 4.

Table 4

Significant analysis of regression model of tillage depth stability

Source of variance	Sum of squares	Degree of freedom	F	P
Model	6.480	6	32.79	<0.01**
x_1	2.670	1	81.00	<0.01**
x_2	1.970	1	59.75	<0.01**
x_3	1.310	1	39.69	<0.01**
x_1x_2	0.157	1	4.79	0.054
x_1x_3	0.235	1	7.14	0.023*
x_2x_3	0.143	1	4.34	0.064
Residual	0.329	10		
Lack-of-fit term	0.293	6	5.29	0.065
Pure errors	0.037	4		
Sum	6.81	16		

Note: ** very significant (P<0.01); * significant (P<0.05)

Analysis of the coefficient of variation of tillage depth stability shows (Table 4) that the pin of the regression model is < 0.01, indicating the model is extremely significant. Specifically, the coefficients of x1, x2, x3, and x1x3 are all significant (P<0.05), and other items are not. The regression equation of the coefficient of variation of tillage depth stability is as follows:

$$y = 5.864 + 0.578x_1 - 0.496x_2 - 0.404x_3 - 0.243x_1x_3 \quad (12)$$

Based on the regression equation, the response surface method (RSM) curves of the stability variation coefficient of tillage depth with respect to tillage speed, tillage depth and spring elastic coefficient are plotted on Design-Expert 12.0. The coefficient of variation of the tillage depth stability gradually increases as the tillage speed increases, and slightly decreases as the tillage depth and the spring elastic coefficient increase (Fig. 14). The contribution rates of different factors to the coefficient of variation of tillage depth stability rank as: tillage speed > tillage depth > spring elastic coefficient.

The experimental data show that in terms of the structural parameters of the obstacle avoidance mechanism, when the tillage speed, tillage depth and spring elastic coefficient are in the working ranges, the coefficient of variation of the tillage depth stability is less than 8%, meeting the design requirements.

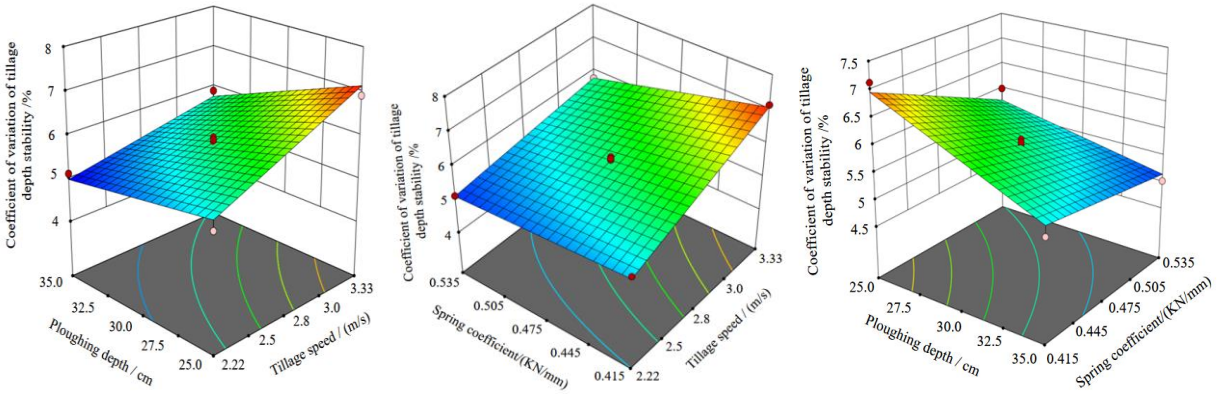

(a) (b) (c)

Fig. 14 - Effect of interaction factors on tillage depth stability

a. Effects of the tillage depth and tillage speed on tillage depth stability

b. Effects of the spring elastic coefficient and tillage speed on tillage depth stability

c. Effects of the tillage depth and spring elastic coefficient on tillage depth stability

The results show that, when the tilling plough makes contact with hard objects, the mechanism can rapidly and effectively start the anti-overload automatic obstacle avoidance device to make the plough pass through hard obstacles. When the plough passes through the obstacles, it can immediately return to its working position, thereby avoiding missing tillage and stopping, and improving the reliability and working performance of the plough device.

CONCLUSIONS

A two-way plough equipment with anti-overload automatic obstacle avoidance mechanism is designed. Its aim is to achieve the anti-overload automatic obstacle avoidance function of a two-way plough equipment during tillage in rocky barren soils. The mechanism can rapidly respond and avoid obstacles such as rocks, and can immediately relocate after passing through the obstacles. Thus, it can improve the reliability, adaptivity and ploughing efficiency of the plough, and further improve the tillage quality in barren soils, creating excellent seedbed conditions for crop growth.

(1) The structure and key parameters of the anti-overload automatic obstacle avoidance mechanism are designed, and the obstacle avoidance motion process is analysed. Its motion equation and quasi-static forced equation are established, and its motion laws and force status are determined. At a safety factor of 1.3, the relation between spring pre-tightening force and plough resistance is clarified. The curves showing how the force of springs with different elastic coefficients changes with the rotation angle of the mechanism are plotted.

(2) A virtual prototype simulation model of the anti-overload automatic obstacle avoidance mechanism is constructed. The motion trajectory curves at the contact point of the plough, the changes in the angular speed of the chord parts during obstacle avoidance, and the changes of spring bounce before and after obstacle avoidance are obtained through ADAMS analysis. The forces of the trolley wheels are analysed. The simulations show that the mechanism can effectively perform obstacle avoidance actions.

(3) The site experiments validated that the mechanism can avoid obstacles at the preset load. Based on Box-Behnken Design of the response surface method, a three-factor scheme involving tillage speed, tillage depth and spring elastic coefficient was designed. The contribution rates of the test factors to the coefficient of variation of the tillage depth stability ranked as tillage speed > tillage depth > spring elastic coefficient. In the case of obstacle overloading, the mechanism can effectively perform obstacle avoidance actions, and the coefficient of variation of its tillage depth stability is less than 8%, meeting the design requirements.

FUNDING

This research was funded by the Xinjiang Corps Regional Innovation Plan (grant no. 2021BB015).

REFERENCES

1. Gao, Z., Fan, Q., Liu, Y., Wang, G., Yang, G., Shi, L., Wang, J., Zeng, S., Chen, Y. (2021). The Current Situation, Existing Problems, and Suggestions of the XPCC's Cultivated Land Quality Protection (兵团耕地质量保护现状、存在问题及建议). *Chinese Journal of Xinjiang Farm Research of Science and Technology*, Vol. *44* (6), pp. 1-5.
2. Guilherme, A.F. C., Renato, P. de L., Maurício, R. C., Ricardo, O. B., Mario, M. R., João, L.N. C., (2021). Machinery traffic in sugarcane straw removal operation: Stress transmitted and soil compaction. *Soil and Tillage Research*, Vol. (213), 105122.
3. Kim, W.S., Kim, Y.J., Park, S.U., Kim, Y.S. (2021). Influence of soil moisture content on the traction performance of a 78-kW agricultural tractor during plow tillage. *Soil and Tillage Research*. Vol. (207), 104851. https://doi.org/10.1016/j.still.2020.104851.
4. Kim, Y. J., Kim, W. S., Sim, T., Yi, S., Choi, Y. S. (2022a). Development of DEM-MBD coupling model for draft force prediction of agricultural tractor with plowing depth. *Computers and Electronics in Agriculture,* Vol. (202), 107405. https://doi.org/10.1016/j.compag.2022.107405.
5. Kim, Y.-S., Lee, S.-D., Baek, S.-M., Baek, S.-Y., Jeon, H.-H., Lee, J.-H., Siddique, M. A. A., Kim, Y.-J., Kim, Sim, W.-S., Yi, S., Choi, Y.-S. (2022b). Development of DEM-MBD coupling model for draft force prediction of agricultural tractor with plowing depth. *Computers and Electronics in Agriculture*, Vol. (202), 107405.
6. Li, Q.C., Zheng X., Meng X., Liu, J., Zhang, L., Liang, Y. (2021). Application status and improvement suggestions of mouldboard plough in the cornfield of Northern Xinjiang. *Journal of Chinese Agricultural Mechanization*, Vol. *42*(7), pp. 202-208.
7. Liu, J., Zheng, X., Meng, X., Tang, Z., Yang, H., Zhang, L. (2021). Current situation and prospect of research on plough surface (铧式犁犁体曲面研究现状与展望). *Journal of Chinese Agricultural Mechanization*, Vol. *42*(3), pp. 13-21+39.

8. Liu, J.B., Zheng, X., Meng, X.J., Yang, H.J., Zhang, L.Y., Li, Q.C. (2022). Analysis and experimental study on plough tillage resistance model（犁体耕作阻力模型仿真分析与试验研究）. *Agricultural Research in the Arid Areas*, Vol. *40* (1), pp. 264-274.
9. Ma, H., Chang, Y. (2020). Flipping plow with overload protection and its overload protection method. China Patent CN110637524A, 3 Jan 2020.
10. Ma, S., Xu, L., Yuan, Q., Niu, C., Wang, S., Yuan, X. (2020). Development of automatic obstacle-avoiding grapevine cold-proof soil cleaners (自动避障式葡萄藤防寒土清土机研制). *Transactions of the Chinese Society of Agricultural Engineering (Transactions of the CSAE)*, Vol. *36* (7), pp. 1-10.
11. Mileusnić, Z. I., Saljnikov, E., Radojević, R. L., Petrović, D. V. (2022). Soil compaction due to agricultural machinery impact. *Journal of Terramechanics*, Vol. (100), pp. 51- 60.
12. Mileusnić, Z.I., Saljnikov, E., Radojević, R. L., Petrović, D. V. (2022). Soil compaction due to agricultural machinery impact. *Journal of Terramechanics*, Vol. (100), pp. 51-60.
13. Naderi-Boldaji, M., Karparvarfard, S. H., Azimi-Nejadian, H. (2023). Investigation of the predictability of mouldboard plough draught from soil mechanical strength (cone index vs. shear strength) using finite element modelling. *Journal of Terramechanics*, Vol. (108), pp. 21-31.
14. Salavat, M., Yakov, L., Ildar, F., Eduard, K., Ildar, R. (2023). Justification of the soil DEM-model parameters for predicting the plow body resistance forces during plowing. *Journal of Terramechanics*, Vol. (109), pp. 37-44.
15. Shafaei, S.M., Loghavi, M., Kamgar, S. (2021). Profound insight into tractor energy dissipation through inevitable interaction inside wheel-soil interface for the period of plowing works. *Soil and Tillage Research*, Vol. (211), 104998.
16. Wang, W.X., Cao, Y.G., Su, R.Q., Qiu, M., Song, L., Zhou, W. (2020). Cultivated land protection policy in China: Background, Effect and future trends (我国耕地保护政策研究:基于背景、效果与未来趋势). *Chinese Journal of Agricultural Resources and Regional Planning*, Vol. *41*(10), pp. 40-51.
17. Wittke, M., Wolf, M., Weigert, F., Darnieder, M., Gerlach, E., Zimmermann, K., Theska, R. (2022). Investigations on a torque-compensating adjustment drive for mechanically sensitive device. European Society for Precision Engineering and Nanotechnology, Conference Proceedings - 22nd International Conference and Exhibition, EUSPEN 2022, Pages 81-82.
18. Zhang, M.Y., Qi, R.F., Wang, Q., Liu, F. (2021a). Design and performance test of obstacle detection system for boom manipulator (喷杆机械臂障碍物检测系统设计与性能测试). *China Agricultural Informatics*, Vol. *33*(2), pp. 49-56.
19. Zhang, S., Ren, W., Xie, B., Luo, Z., Wen, C., Chen, Z., Zhu, Z., Li, T. (2023). A combined control method of traction and ballast for an electric tractor in ploughing based on load transfer. *Computers and Electronics in Agriculture*, Vol. (207), 107750.
20. Zhang, W.F., Yang, S.Q., Lou, S., Jin, Y.H., Liu, P. (2020). Effects of tillage methods and straw mulching on the root distribution and yield of summer maize (耕作方式与秸秆覆盖对夏玉米根系分布及产量的影响). *Transactions of the Chinese Society of Agricultural Engineering (Transactions of the CSAE)*, Vol. *36*(7), pp. 117-124.
21. Zhang, W.K. (2021b). Study on Active Barrier Control System of Breaker Device Based on ADRC (基于 ADRC 的破茬装置主动避障控制系统研究). Kunming University of Science and Technology. (In Chinese)